

Nanoscale

Accepted Manuscript



This is an *Accepted Manuscript*, which has been through the Royal Society of Chemistry peer review process and has been accepted for publication.

Accepted Manuscripts are published online shortly after acceptance, before technical editing, formatting and proof reading. Using this free service, authors can make their results available to the community, in citable form, before we publish the edited article. We will replace this *Accepted Manuscript* with the edited and formatted *Advance Article* as soon as it is available.

You can find more information about *Accepted Manuscripts* in the [Information for Authors](#).

Please note that technical editing may introduce minor changes to the text and/or graphics, which may alter content. The journal's standard [Terms & Conditions](#) and the [Ethical guidelines](#) still apply. In no event shall the Royal Society of Chemistry be held responsible for any errors or omissions in this *Accepted Manuscript* or any consequences arising from the use of any information it contains.

COMMUNICATION

Broadband Ultrafast Nonlinear Absorption and Nonlinear Refraction of Layered Molybdenum Dichalcogenide Semiconductors

Cite this: DOI: 10.1039/x0xx00000x

Received 00th January 2012,
Accepted 00th January 2012

DOI: 10.1039/x0xx00000x

www.rsc.org/

Kangpeng Wang,^{a, b} Yanyan Feng,^a Chunxia Chang,^a Jingxin Zhan,^a Chengwei Wang,^c Quanzhong Zhao,^c Jonathan N. Coleman,^b Long Zhang,^{a*} Werner J. Blau^{a, b} and Jun Wang^{a, c*}

A series of layered molybdenum dichalcogenides, i.e., MoX₂ (X=S, Se and Te) were prepared in cyclohexylpyrrolidinone by liquid-phase exfoliation technique. High quality of the two-dimensional nanostructures was verified by transmission electron microscopy and absorption spectroscopy. Open- and closed-aperture Z-scans were employed to study the nonlinear absorption and nonlinear refraction of the MoX₂ dispersions, respectively. All the three layered nanostructures exhibit prominent ultrafast saturable absorption (SA) for both femtosecond (fs) and picosecond (ps) laser pulses over a broad wavelength range from the visible to the near infrared. While the dispersions treated with low speed centrifugation (1500 rpm) have SA response, the MoS₂ and MoSe₂ dispersions after higher speed centrifugation (10000 rpm) possess two-photon absorption for fs pulses at 1030 nm, which is due to the significant reduction of average thickness of the nanosheets, and hence the broadening of bandgap. In addition, all dispersions show obvious nonlinear self-defocusing for ps pulses at both 1064 nm and 532 nm, resulting from the thermally induced nonlinear refractive index. The versatile ultrafast nonlinear properties imply a huge potential of the layered MoX₂ semiconductors in the development of nanophotonic devices, such as mode-lockers, optical limiters, optical switches, etc.

Introduction

Owing to the specific two-dimensional (2D) confinement of electron motion and the absence of interlayer perturbation, layered 2D crystals of semiconducting transition metal dichalcogenides (TMDs) are considered as promising materials for emerging applications in nano-electronic, micromechanic, and nano-optoelectronic devices with high performance and unique functions.¹⁻⁵ The TMD materials such as MoX₂ and WX₂ (X=S, Se, Te) possess similar lattice structures and show layer-dependent property, e.g., indirect to direct bandgap transition as the decreasing of the number of monolayer.^{1, 6-9} So far, a series of photonic properties, such as, visible photoluminescence, transient absorption, second harmonic generation, third harmonic generation, etc. have been demonstrated in 2D TMD structures.¹⁰⁻¹⁶ We recently reported for the first time, to the best of our knowledge, the prominent ultrafast saturable absorption (SA) performance in layered MoS₂ nanosheets in the near infrared (NIR) region.¹⁷ These extraordinary photonic properties open up the door to TMD-based nano-photonic devices, such as optical switches, pulse shaping devices, mode-lockers, optical limiters, etc., capable of ultrafast response and broadband tenability.¹⁷⁻²⁰

For the sake of developing high performance photonic devices, it is undoubtedly important to have a comprehensive understanding on the fundamental ultrafast and nonlinear optical (NLO) properties of the working substances. In this work, a series of dispersions containing a large population of pristine molybdenum dichalcogenide nanosheets were dispersed in cyclohexylpyrrolidinone (CHP) by high yield liquid-exfoliation (LPE) technique.²¹⁻²³ The absorption spectroscopy and transmission electron microscope (TEM) characterizations showed high quality of the layered nanostructures. We study systematically the nonlinear absorption and nonlinear refraction properties of the layered MoX₂ nanostructures by Z-scan over a broad temporal (ps-fs) and spectral (Vis-NIR) range.

Results and discussion

The liquid exfoliation has been proved to be a simple, effective and productive technique to exfoliate layered TMD crystals and prepare high-quality 2D nanostructures.²¹⁻²³ Stable dispersions of layered TMD materials can be obtained, provided that the surface energy of solvent matches well with that of layered materials. In this work, CHP was utilized to disperse MoS₂,

MoTe₂, and MoSe₂, respectively. The initial dispersions were treated for 60 min by a high-power sonication tip. After sonication, the dispersions were allowed to settle for ~24 h before centrifuging to remove large sedimentations. The top two-thirds of the dispersions was collected after the centrifugation at 1500 rpm for 90 min. All dispersions are stable against sedimentation and no further aggregation for a period of weeks (See Fig. S1).

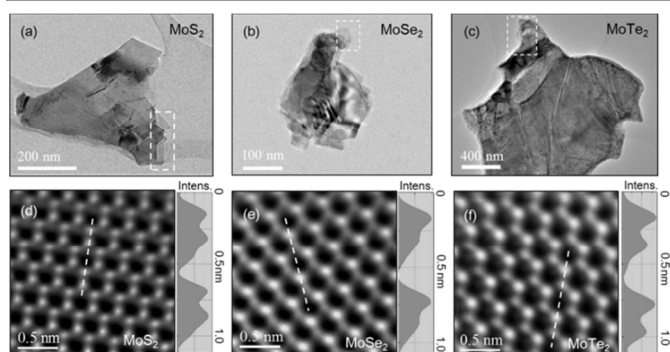


Fig. 1 TEM images of layered MoS₂, MoSe₂, MoTe₂ nanoflakes. (a)-(c) Overviews of the nanoflakes. (d)-(f) High-magnification TEM images of the few-layer nanosheets. Right-side graphs are intensity distribution along the dash lines.

In general, the MoX₂ dispersions prepared by LPE are composed of monolayers and few-layers.^{21, 23} TEM was employed to confirm the status of the dispersed nanosheets. The specimens were prepared by dropping a few milliliters of each dispersion on copper holey carbon grids (mesh size 400). Low-magnification TEM images of typical flakes in the three dispersions are shown in Fig. 1 (a)-(c). It appears that most of the nanosheets in the three dispersions are few-layer flakes. At the edge of the nanosheets, very few-layer structures can be seen, as indicated by the dash boxes in Fig. 1 (a)-(c). Fig. 1 (d)-(f) show high-magnification images from the nanosheet edges located in the dash boxes. All the HRTEM images were firstly processed by fast Fourier transform with digital periodic filter, then inverse fast Fourier transform to get images for lower noise and better clearance of atoms. The fine atomic structures of MoS₂, MoSe₂, and MoTe₂, together with electron diffraction patterns (See Fig. S2), imply that the 2H structures of molybdenum dichalcogenides remain undistorted after LPE preparation.^{21, 23} The pixel intensity distributions along the neighboring atoms are illustrated on the right-side of Fig. 1 (d)-(f). The number of monolayer of the nanosheets could be roughly deduced by the pixel intensity analyze of the neighboring atoms.²¹ As for MoS₂ in Fig. 1(d), the neighboring atoms show similar intensity, while for MoSe₂ and MoTe₂, neighboring atoms appear to be high contrast in intensity. Therefore, the MoS₂ nanosheet in Fig. 1(d) seems to have even number of monolayer, while MoSe₂ and MoTe₂ appear very likely to be monolayer or triple-layers. Nonetheless, the dispersions used in this work were dominated by multilayer nanosheets.

Absorption spectroscopic characterization was carried out for the three MoX₂ dispersions. As shown in Fig. 2, the absorption spectra are comparable to the previous works,²² confirming the existence of high-quality nanosheets in dispersions. It is seen clearly that the characteristic A and B exciton peaks of MoS₂ and MoSe₂, originating from the interband excitonic transition at the K point, are located at 673 nm (1.84 eV) & 612 nm (2.03 eV) and 810 nm (1.53 eV) & 708 nm (1.75 eV), respectively, indicating a pristine 2H poly-

type.^{24, 25} Referring to the relationship between exciton energy of A peak and the thickness of MoS₂ nanosheets, one can estimate the average thickness of the nanosheets in the MoS₂ dispersions to be > 8 nm, equivalent to ~15 monolayers.¹⁰

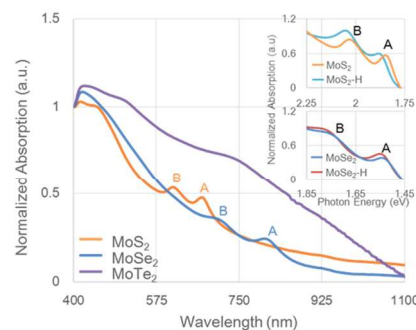


Fig. 2 Absorption spectra of the MoX₂ dispersions. Insets: Shift of the A and B exciton peaks for the MoS₂ and MoSe₂ dispersions with a low speed centrifugation treatment (MoX₂) and higher speed treatment (MoX₂-H).

Open-aperture (OA) and closed-aperture (CA) Z-scans were employed to study the nonlinear absorption and nonlinear refraction of the MoX₂ dispersions, respectively.^{17, 26-28} The OA Z-scan measures the total transmittance through the sample as a function of incident laser intensity, while the sample is sequentially moved through the focus of a lens (along the z-axis). The optical setup was analogous to that used in the previous experiments in measuring NLO response of nanomaterials.^{17, 29, 30} For the CA Z-scan, an aperture was placed right after the sample dispersions to confine the transmitted beam incident on detector. With the help of Z-scan, the dispersions were characterized by using the laser sources with different wavelength and pulse duration parameters, i.e., 1 KHz, 100 fs pulses at 800 nm from a Ti: Sapphire mode-lock laser, 0.1 KHz, 340 fs pulses at 1030 nm and its second harmonic, 515 nm, from a chirped pulse amplified fiber laser, and 10 KHz, 100 ps pulses at 1064 nm and 532 nm from a ps fiber laser. During the measurements, unwanted NLO effects, such as, supercontinuum generation from the solvent CHP, nonlinear scattering, etc., have been carefully avoided by using the low intensity pulses and employing the pure CHP for reference testing. Fig. 3 and 4 show the typical Z-scan results for fs and ps lasers, respectively.

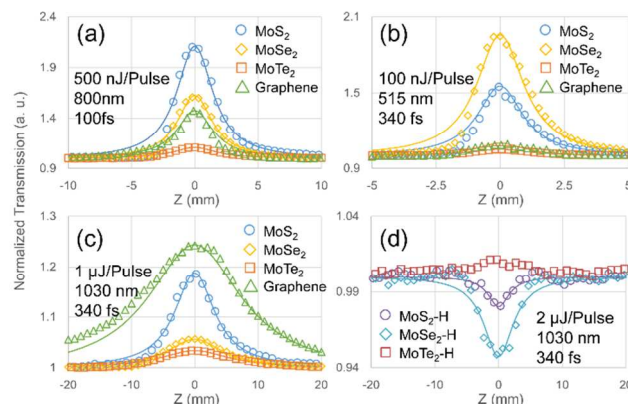


Fig. 3 OA Z-scan results of the MoX₂ dispersions in fs region. Samples in (a)-(c) exhibit obvious SA response, while showing TPA response in (d) for the MoS₂ and MoSe₂ dispersions with a higher speed centrifugation treatment (10000 rpm).

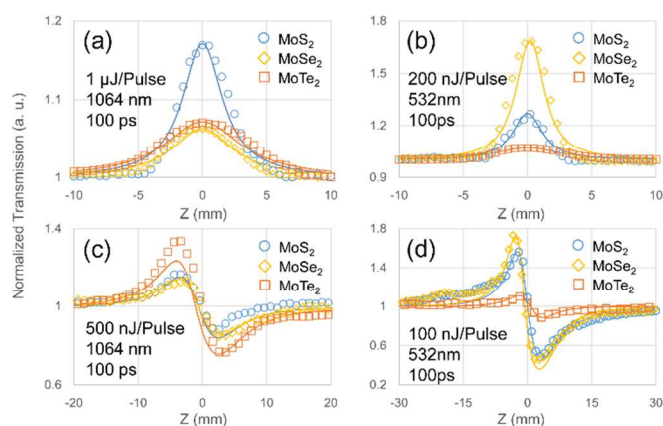


Fig. 4 Z-scan results of the MoX₂ dispersions for the ps pulses. (a)–(b) OA Z-scan results at 1064 nm and 532 nm. (c)–(d) CA Z-scan results. All of the dispersions exhibit self-defocusing shape.

As shown in Figs. 3(a)–(c) and 4(a)–(b), all the three molybdenum dichalcogenides, MoS₂, MoSe₂ and MoTe₂, exhibit obvious saturable absorption response from the visible (515 and 532 nm) to NIR (800, 1030 and 1064 nm) for both fs and ps pulses with various repetition rates (0.1, 1, and 10 KHz), implying a broadband ultrafast NLO performance. The molybdenum dichalcogenides are well-known for the unique bandgap transition from indirect to direct when the layered structure reduces from bulk to monolayer. The indirect bandgaps for the multilayer MoS₂, MoSe₂ and MoTe₂, were determined to be 1.2 eV (1033 nm), 1.1 eV (1128 nm) and 1.0 eV (1239 nm), respectively. In contrast, the direct bandgaps for the monolayer MoX₂ are increased to 1.8 eV (690 nm), 1.5 eV (828 nm) and 1.1 eV (1128 nm), respectively.¹ In general, semiconductors with the bandgap smaller than the incident photon energy exhibit saturable absorption, resulting from the free-carrier excitation from valence band to conduction band, and hence Pauli-blocking. However, photons with energy less than bandgap will not be able to excite electrons/holes to conduction/valence band directly, unless two photons are absorbed simultaneously, i.e., two-photon absorption (TPA) takes place. In contrast to SA, TPA results in the normalized transmission decreases when the incident intensity increases, leading to a valley centered at the focal point in Z-scan curve.

Laser pulses at 515 and 532 nm can induce SA for the MoS₂ monolayer with the bandgap of ~1.8 eV (~690 nm), while pulses at 800, 1030, and 1064 nm are able to generate TPA. In contrast, the few-layer MoS₂ with the bandgap of ~1.2 eV (~1033 nm) exhibit SA for all wavelengths used in this work. SA responses in Figs. 3(a)–(c) and 4(a)–(b) are attributed to the domination of few-layer nanosheets in the dispersions. TPA from the minority monolayers would be screened by the strong SA in the majority few-layers, as we predicted in the previous work.³¹ Similarly, by comparing the bandgaps of few-layer MoSe₂ and MoTe₂ with the incident photon energies, it is undoubtedly that the MoSe₂ and MoTe₂ dispersions possess SA to all of the laser pulses. Although photon energy for pulses at 1064 nm is slightly less than the theoretical prediction of bandgap for the few-layer MoS₂, absorption saturation was still observed in the MoS₂ dispersions, which was also reported by other groups.^{18, 19} The possible reason may be that there is a small difference between the theoretical and practical bandgap, or defect induced interband states.

Nonlinear absorption coefficient α_{NL} can be deduced by numerically fitting the Z-scan curves with the nonlinear

propagation equation $\frac{dI}{dz} = -(\alpha_0 + \alpha_{NL}I)I$, in combination of the Gaussian field approximation after the laser beam was focused by the convex lens.^{26, 27} The imaginary part of the third-order NLO susceptibility, $Im\chi^{(3)}$, is directly related to α_{NL} by $Im\chi^{(3)} = \left[\frac{10^{-7}c\lambda n^2}{96\pi^2}\right]\alpha_{NL}$, where c , λ , and n are the light speed in vacuum, wavelength of the laser pulses, and the refractive index, respectively. In order to eliminate the discrepancy caused by the linear absorption α_0 , we define a figure of merit (FOM) for the third-order optical nonlinearity as $FOM = |Im\chi^{(3)}/\alpha_0|$. To obtain the saturable intensity I_s , one can use the propagation equation in the form of $\frac{dI}{dz} = -\frac{\alpha_0 I}{1+I/I_s}$.

All linear and NLO parameters deduced from Figs. 3(a)–(c) and 4(a)–(b) are summarized in Table 1. Since α_0 of each dispersion used in the experiment is different, we mainly adopt FOM as criterion to evaluate the SA performance of the materials. The use of FOM also helps us to compare with the other nanomaterials reported.^{32–35}

Referring to FOM for fs pulses in Table 1, overall, the MoX₂ nanosheets exhibit more pronounced SA response than graphene. At 1030 nm, FOMs for all the three MoX₂ have the same magnitude of 10^{-15} esu cm. FOMs of MoS₂ and MoTe₂ are larger than those of MoSe₂ and graphene by one order of magnitude at 800 nm, and the comparison between MoS₂ and graphene consists with the previous results.³¹ At the above two wavelengths, MoTe₂ shows the largest FOM among the four dispersions. At 515 nm, FOMs of all the three MoX₂ dispersions exceed that of graphene by one order of magnitude, and MoSe₂ turns out to be the material possessing the largest FOM. It should be mentioned that we have found the similar regularity by analyzing the saturation intensity I_s presented in Table 1. Graphene dispersions exhibit the largest I_s in comparison with all the MoX₂ dispersions. MoTe₂ dispersions show the lowest I_s at both 800 and 1030 nm, while I_s of MoSe₂ is minimum at 515 nm. It is noticed that FOM of the MoX₂ in ps regime is greater than that in fs regime by two orders of magnitude. For instance, FOM of MoS₂ for 340 fs pulses at 1030 nm is $\sim 10^{-15}$ esu cm, which becomes $\sim 10^{-13}$ esu cm for 100 ps pulses at 1064 nm. MoSe₂ and MoTe₂ nanosheets in dispersions exhibit the largest FOM at 1064 nm and 532 nm, respectively. Overall, the LPE prepared MoX₂ dispersions are shown to be promising broadband ultrafast SA materials. Due to the relative narrow bandgap of ~1.0 eV, the few-layer MoTe₂ nanosheets show the best SA performance, i.e., the largest FOM and the lowest I_s at NIR, implying a potential as a passive mode-locker working for up to ~1239 nm.

To investigate the dependence of the nonlinear response on the nanosheet size and hence bandgap, we prepared another batch of MoX₂ dispersions, which is termed as ‘MoX₂-H’ (i.e., MoS₂-H, MoSe₂-H and MoTe₂-H). The MoX₂-H samples were dispersed by CHP as well, with the same procedure as the previous, except that the centrifugation speed was increased to 10,000 rpm. As illustrated in the insets of Fig. 2, A and B exciton peaks of the MoS₂-H and MoSe₂-H dispersions show a clear blue shift. The A exciton peak moves to 663 nm (~1.87 eV) and 806 nm (~1.54 eV) for MoS₂-H and MoSe₂-H, respectively. From the A exciton position, one can deduce an average thickness of the MoS₂-H nanosheets to be ~4 nm (equivalent to ~6 monolayers),¹⁰ which is much less than that in the MoS₂ dispersions with 1500 rpm (> 8 nm). Since there is a distribution for nanosheets with different thicknesses in the LPE prepared dispersions,^{21, 23} the smaller average thickness implies a higher percentage of mono- and few-layers out of all nanosheets in a dispersion. It is likely that the H-series

COMMUNICATION

Table 1 Linear and NLO parameters of the three molybdenum dichalcogenide dispersions measured by OA Z-scan.

Laser	Sample	T (%)	α_0 (cm ⁻¹)	NLO Response	α_{NL} (cm/GW)	$\text{Im}\chi^{(3)}$ (esu)	FOM (esu cm)	I_s (GW/cm ²)
1030 nm, 1 KHz, 340 fs	MoS ₂	30.9	11.75	SA	$-(9.17 \pm 2.56) \times 10^{-2}$	$-(6.7 \pm 1.9) \times 10^{-14}$	$(5.7 \pm 1.6) \times 10^{-15}$	114 ± 63
	MoSe ₂	80.9	2.11	SA	$-(1.29 \pm 0.13) \times 10^{-2}$	$-(9.4 \pm 1.0) \times 10^{-15}$	$(4.22 \pm 0.27) \times 10^{-15}$	121 ± 22
	MoTe ₂	90.6	0.87	SA	$-(7.50 \pm 0.47) \times 10^{-3}$	$-(5.50 \pm 0.34) \times 10^{-15}$	$(6.38 \pm 0.39) \times 10^{-15}$	68 ± 8
	Graphene	18.1	17.10	SA	$-(9.40 \pm 3.18) \times 10^{-2}$	$-(6.9 \pm 2.3) \times 10^{-14}$	$(4.03 \pm 1.36) \times 10^{-15}$	170 ± 51
800 nm, 1 KHz, 100 fs	MoS ₂	32.6	11.22	SA	$-(2.42 \pm 0.80) \times 10^{-2}$	$-(1.38 \pm 0.45) \times 10^{-14}$	$(1.23 \pm 0.40) \times 10^{-15}$	381 ± 346
	MoSe ₂	45.3	7.93	SA	$-(2.54 \pm 0.60) \times 10^{-3}$	$-(1.45 \pm 0.34) \times 10^{-15}$	$(6.9 \pm 1.6) \times 10^{-16}$	590 ± 225
	MoTe ₂	86.3	1.47	SA	$-(3.7 \pm 1.2) \times 10^{-3}$	$-(2.13 \pm 0.66) \times 10^{-15}$	$(1.45 \pm 0.45) \times 10^{-15}$	217 ± 11
	Graphene	16.8	17.85	SA	$-(1.52 \pm 0.42) \times 10^{-2}$	$-(8.7 \pm 2.4) \times 10^{-15}$	$(4.9 \pm 1.4) \times 10^{-16}$	583 ± 127
515 nm, 1 KHz, 340 fs	MoS ₂	7.94	25.34	SA	$-(0.357 \pm 0.064)$	$-(1.31 \pm 0.23) \times 10^{-13}$	$(5.16 \pm 0.92) \times 10^{-15}$	58 ± 21
	MoSe ₂	19.38	16.41	SA	$-(0.245 \pm 0.028)$	$-(9.0 \pm 1.0) \times 10^{-14}$	$(5.46 \pm 0.62) \times 10^{-15}$	43 ± 2
	MoTe ₂	87.60	1.32	SA	$-(1.42 \pm 0.03) \times 10^{-2}$	$-(5.20 \pm 0.12) \times 10^{-15}$	$(3.93 \pm 0.09) \times 10^{-15}$	58 ± 11
	Graphene	13.61	19.94	SA	$-(4.8 \pm 1.3) \times 10^{-2}$	$-(1.75 \pm 0.47) \times 10^{-14}$	$(8.8 \pm 2.3) \times 10^{-16}$	473 ± 219
1064 nm, 10 KHz, 100 ps	MoS ₂	31.30	11.62	SA	$-(5.5 \pm 1.3)$	$-(4.18 \pm 0.98) \times 10^{-12}$	$(3.60 \pm 0.84) \times 10^{-13}$	2.1 ± 0.8
	MoSe ₂	83.01	1.86	SA	$-(2.05 \pm 0.17)$	$-(1.55 \pm 0.13) \times 10^{-12}$	$(8.33 \pm 0.69) \times 10^{-12}$	0.71 ± 0.07
	MoTe ₂	89.88	1.07	SA	$-(2.99 \pm 0.52)$	$-(2.27 \pm 0.39) \times 10^{-12}$	$(2.12 \pm 0.38) \times 10^{-12}$	0.19 ± 0.04
532 nm, 10 KHz, 100 ps	MoS ₂	7.65	25.70	SA	$-(26.2 \pm 8.8)$	$-(9.9 \pm 3.3) \times 10^{-12}$	$(3.9 \pm 1.3) \times 10^{-13}$	1.13 ± 0.52
	MoSe ₂	21.12	15.55	SA	$-(35.6 \pm 8.0)$	$-(1.35 \pm 0.30) \times 10^{-11}$	$(8.7 \pm 2.0) \times 10^{-13}$	0.39 ± 0.16
	MoTe ₂	85.14	1.61	SA	$-(5.54 \pm 0.72)$	$-(2.10 \pm 0.27) \times 10^{-12}$	$(1.30 \pm 0.17) \times 10^{-12}$	0.23 ± 0.03
1030 nm, 1 KHz, 340 fs	MoS ₂ -H	96.61	0.03446	TPA	$(8.0 \pm 1.4) \times 10^{-5}$	$(5.8 \pm 1.0) \times 10^{-17}$	$(1.69 \pm 0.30) \times 10^{-15}$	N/A
	MoSe ₂ -H	96.33	0.03744	TPA	$(2.00 \pm 0.37) \times 10^{-4}$	$(1.47 \pm 0.27) \times 10^{-16}$	$(3.93 \pm 0.72) \times 10^{-15}$	N/A
	MoTe ₂ -H	99.95	0.00050	N/A	N/A	N/A	N/A	N/A

dispersions contain a higher percentage of MoX₂ nanosheets with thinner layers, in comparison with the dispersions after the lower speed centrifugation treatment.

OA Z-scan was conducted for the MoX₂-H dispersions under the 1030 nm, 340 fs laser pulses irradiation, and the results are illustrated in Fig. 3(d). Due to the low nanosheet concentration in MoX₂-H dispersions, the 10 mm long path-length cuvettes were employed to enhance the NLO signal. In opposite to the SA response for the MoX₂ dispersions, Z-scan curves for the MoS₂-H and MoSe₂-H dispersions exhibit a valley around the focal point. The valley-like response is attributed to TPA of the very-few-layer MoX₂ nanosheets. The bandgaps of the very-few-layer MoS₂ and MoSe₂ are much larger than the photon energy of laser pulses at 1030 nm (~1.2 eV). High percentage of the very-few-layer nanosheets in the MoX₂-H dispersions results in the domination of TPA process over SA. In the experiment, we did not observe any NLO response from the MoTe₂-H dispersions, which is probably due to its low content of nanosheets, say, nearly 100% linear optical transmittance (See Table 1). $\text{Im}\chi^{(3)}$ of MoS₂-H and MoSe₂-H are determined to be $(5.84 \pm 1.04) \times 10^{-17}$ and $(1.47 \pm 0.27) \times 10^{-16}$ esu.

A Z-scan was performed to measure the nonlinear refractive index of the three MoX₂ dispersions with the ps and fs laser sources. Using the ps pulses, we observed obvious nonlinear self-defocusing signal from all dispersions including graphene. The CA Z-scan results for the MoX₂ dispersions at 532 and 1064 nm are showed in Fig. 4 (c)-(d). The results for graphene dispersions are given in Fig. S3. For the fs pulses, there is no any measurable CA signal from all the samples. Intensity dependent NLO refractive index can be described by $n = n_0 + n_2 I$, where n_0 is the refractive index of medium and n_2 is the NLO refractive index, which can be estimated by fitting the CA Z-scan results using the model mentioned in literature.³⁶ The real part of third-order NLO susceptibility $\text{Re}\chi^{(3)}$ and n_2 have the relation of $\text{Re}\chi^{(3)}$ (esu) = $\frac{n_0^2 c}{12\pi^2} n_2 \left(\frac{\text{cm}^2}{W}\right)$. Based on the equations, we calculated n_2 and $\text{Re}\chi^{(3)}$ parameters given in Table 2. Since the thermally-induced nonlinear refractive index change cannot be neglected if the pulse duration is larger than ~30 ps and no CA signal observed in fs region, it is likely that the self-defocusing results from the thermally induced NLO index.³⁷ The MoX₂ nanosheets absorb laser energy, and then transform it to heat, resulting in thermal expansion and refractive index change of the whole dispersions. In contrast to

the longer ps pulses, the fs pulses have much lower average power to deposit, leading to weakly unmeasurable thermally induced NLO effect. It should be mentioned that we did not observe any significant CA signal from CHP except for the ps pulses at 1064 nm. However, the NLO effect of CHP was still much less than that of the MX₂ dispersions. $\text{Re}\chi^{(3)}$ of CHP was determined to be $-(1.07 \pm 0.08) \times 10^{-12}$ esu at 1064 nm.

Table 2 NLO refractive parameters of the MoX₂ dispersions in ps region.

Laser	Sample	α_0 (cm ⁻¹)	n_2 (cm ² /W) $\times 10^{-12}$	$\text{Re}\chi^{(3)}$ (esu) $\times 10^{-11}$
1064 nm, 10 KHz, 100 ps	MoS ₂	11.62	$-(0.207 \pm 0.021)$	$-(1.18 \pm 0.12)$
	MoSe ₂	1.86	$-(0.120 \pm 0.003)$	$-(0.682 \pm 0.018)$
	MoTe ₂	1.07	$-(0.160 \pm 0.027)$	$-(0.92 \pm 0.15)$
	Graphene	19.46	-13.7	-78.2
532 nm, 10 KHz, 100 ps	MoS ₂	25.70	$-(2.5 \pm 1.2)$	$-(14.1 \pm 6.5)$
	MoSe ₂	15.55	$-(1.82 \pm 0.73)$	$-(10.3 \pm 4.2)$
	MoTe ₂	1.61	$-(0.11 \pm 0.04)$	$-(0.62 \pm 0.21)$
	Graphene	19.45	-2.34	-13.3

Conclusions

The NLO responses of the MoS₂, MoSe₂, and MoTe₂ dispersions prepared by LPE in CHP have been extensively investigated by employing Z-scan technique for fs and ps pulses from the visible to NIR. All the three MoX₂ dispersions dominated by few-layer nanosheets show evident broadband SA response, and their FOMs exceed that of graphene in fs region at 515, 800, and 1030 nm. The nonlinear responses in ps region seem to be much stronger than that in fs region. In addition, the dispersions of MoS₂ and MoSe₂ prepared by higher speed centrifugation exhibit TPA for fs pulses at 1030 nm. The versatile ultrafast NLO properties of the layered MoX₂ imply a huge potential in the development of nanophotonic devices, such as mode-lockers, optical limiters, optical switches, etc.

Acknowledgements

This work is supported in part by the National Natural Science Foundation of China (No. 61178007, No. 61308034), Science and Technology Commission of Shanghai Municipality (No. 12ZR1451800, Nano Project No. 11nm0502400, Shanghai Pujiang Program 12PJ1409400, and the Excellent Academic Leader of Shanghai No. 10XD1404600). J.N.C. is supported by the ERC Grant SEMANTICS. W.J.B. is supported in part by Science Foundation Ireland (No. 12/IA/1306). J.W. thanks the financial supports from the National 10000-Talent Program, CAS 100-Talent Program.

Notes and references

a Key Laboratory of Materials for High-Power Laser, Shanghai Institute of Optics and Fine Mechanics, Chinese Academy of Sciences, Shanghai 201800, China.

b School of Physics and the Centre for Research on Adaptive Nanostructures and Nanodevices (CRANN), Trinity College Dublin, Dublin 2, Ireland

c State Key Laboratory of High Field Laser Physics, Shanghai Institute of Optics and Fine Mechanics, Chinese Academy of Sciences, Shanghai 201800, China

Electronic Supplementary Information (ESI) available: Electron scattering patterns from TEM characterizations of MX₂ nanosheets; CA

Z-scan results of graphene dispersions in ps region. See DOI: 10.1039/b000000x/

- Q. H. Wang, K. Kalantar-Zadeh, A. Kis, J. N. Coleman and M. S. Strano, *Nature Nanotechnology*, 2012, 7, 699-712.
- R. Mas-Balleste, C. Gomez-Navarro, J. Gomez-Herrero and F. Zamora, *Nanoscale*, 2011, 3, 20-30.
- S. Z. Butler, S. M. Hollen, L. Cao, Y. Cui, J. A. Gupta, H. R. Gutierrez, T. F. Heinz, S. S. Hong, J. Huang and A. F. Ismach, *ACS Nano*, 2013, 7, 2898-2926.
- D. Jariwala, V. K. Sangwan, L. J. Lauhon, T. J. Marks and M. C. Hersam, *ACS nano*, 2014.
- J.-W. Jiang, H. Park and T. Rabczuk, *Nanoscale*, 2014.
- W. Jin, P.-C. Yeh, N. Zaki, D. Zhang, J. T. Sadowski, A. Al-Mahboob, A. M. van der Zande, D. A. Chenet, J. I. Dadap and I. P. Herman, *Physical Review Letters*, 2013, 111, 106801.
- K. F. Mak, C. Lee, J. Hone, J. Shan and T. F. Heinz, *Physical Review Letters*, 2010, 105, 136805.
- W. Zhao, Z. Ghorannevis, L. Chu, M. Toh, C. Kloc, P.-H. Tan and G. Eda, *ACS Nano*, 2012, 7, 791-797.
- Y. Zhang, T.-R. Chang, B. Zhou, Y.-T. Cui, H. Yan, Z. Liu, F. Schmitt, J. Lee, R. Moore and Y. Chen, *Nature Nanotechnology*, 2014, 9, 111.
- G. Eda, H. Yamaguchi, D. Voiry, T. Fujita, M. Chen and M. Chhowalla, *Nano Letters*, 2011, 11, 5111-5116.
- V. Štengl and J. Henych, *Nanoscale*, 2013, 5, 3387-3394.
- H. Shi, R. Yan, S. Bertolazzi, J. Brivio, B. Gao, A. Kis, D. Jena, H. G. Xing and L. Huang, *ACS Nano*, 2013, 7, 1072-1080.
- N. Kumar, Q. Cui, F. Ceballos, D. He, Y. Wang and H. Zhao, *Nanoscale*, 2014.
- A. Splendiani, L. Sun, Y. Zhang, T. Li, J. Kim, C.-Y. Chim, G. Galli and F. Wang, *Nano Letters*, 2010, 10, 1271-1275.
- R. Wang, H.-C. Chien, J. Kumar, N. Kumar, H.-Y. Chiu and H. Zhao, *ACS Applied Materials & Interfaces*, 2013.
- N. Kumar, S. Najmaei, Q. Cui, F. Ceballos, P. M. Ajayan, J. Lou and H. Zhao, *Physical Review B*, 2013, 87, 161403.
- K. Wang, J. Wang, J. Fan, M. Lotya, A. O'Neill, D. Fox, Y. Feng, X. Zhang, B. Jiang and Q. Zhao, *ACS Nano*, 2013, 7, 9260-9267.
- H. Zhang, S. Lu, J. Zheng, J. Du, S. Wen, D. Tang and K. Loh, *Optics Express*, 2014, 22, 7249-7260.
- S. Wang, H. Yu, H. Zhang, A. Wang, M. Zhao, Y. Chen, L. Mei and J. Wang, *Advanced Materials*, 2014.
- D.-S. Tsai, K.-K. Liu, D.-H. Lien, M.-L. Tsai, C.-F. Kang, C.-A. Lin, L.-J. Li and J.-H. He, *ACS Nano*, 2013, 7, 3905-3911.
- J. N. Coleman, M. Lotya, A. O'Neill, S. D. Bergin, P. J. King, U. Khan, K. Young, A. Gaucher, S. De and R. J. Smith, *Science*, 2011, 331, 568-571.
- G. Cunningham, M. Lotya, C. S. Cucinotta, S. Sanvito, S. D. Bergin, R. Menzel, M. S. Shaffer and J. N. Coleman, *ACS Nano*, 2012, 6, 3468-3480.
- V. Nicolosi, M. Chhowalla, M. G. Kanatzidis, M. S. Strano and J. N. Coleman, *Science*, 2013, 340.
- R. Bromley, R. Murray and A. Yoffe, *Journal of Physics C: Solid State Physics*, 1972, 5, 759.
- A. Beal, J. Knights and W. Liang, *Journal of Physics C: Solid State Physics*, 1972, 5, 3540.

26. M. Sheik-Bahae, A. A. Said, T.-H. Wei, D. J. Hagan and E. W. Van Stryland, *Quantum Electronics*, IEEE Journal of, 1990, 26, 760-769.
27. M. Sheik-Bahae, A. A. Said and E. W. Van Stryland, *Optics Letters*, 1989, 14, 955-957.
28. H. Yan and J. Wei, *Photonics Research*, 2014, 2, 51-58.
29. J. Wang, Y. Hernandez, M. Lotya, J. N. Coleman and W. J. Blau, *Advanced Materials*, 2009, 21, 2430-2435.
30. J. Li, H. Guo and Z.-y. Li, *Photonics Research*, 2013, 1, 28-41.
31. K. Wang, J. Wang, J. Fan, M. Lotya, A. O'Neill, D. Fox, Y. Feng, X. Zhang, B. Jiang, Q. Zhao, H. Zhang, J. N. Coleman, L. Zhang and W. J. Blau, *ACS Nano*, 2013, 7, 9260-9267.
32. S. Kumar, M. Anija, N. Kamaraju, K. Vasu, K. Subrahmanyam, A. Sood and C. Rao, *Applied Physics Letters*, 2009, 95, 191911.
33. S. Kumar, N. Kamaraju, K. Vasu, A. Nag, A. Sood and C. Rao, *Chemical Physics Letters*, 2010, 499, 152-157.
34. H. I. Elim, W. Ji, M.-T. Ng and J. J. Vittal, *Applied Physics Letters*, 2007, 90, 033106.
35. H. I. Elim, J. Yang, J.-Y. Lee, J. Mi and W. Ji, *Applied Physics Letters*, 2006, 88, 083107.
36. C. H. Kwak, Y. L. Lee and S. G. Kim, *JOSA B*, 1999, 16, 600-604.
37. R. W. Boyd, Elsevier Science, 3 edn., 2010, ch. 4, p. 240